Development of Soil-Suppressed Impervious Surface Area Index for Automatic Urban Mapping

Akib Javed, Zhenfeng Shao, Iffat Ara, Muhammad Nasar Ahmad, Md. Enamul Huq, Nayyer Saleem, and Fazlul Karim

Abstract

Expanding urban impervious surface area (ISA) mapping is crucial to sustainable development, urban planning, and environmental studies. Multispectral ISA mapping is challenging because of the mixed-pixel problems with bare soil. This study presents a novel approach using spectral and temporal information to develop a Soil-Suppressed Impervious Surface Area Index (SISAI) using the Landsat Operational Land Imager (OLI) data set, which reduces the soil but enhances the ISA signature. This study mapped the top 12 populated megacities using SISAI and achieved an overall accuracy of 0.87 with an F1-score of 0.85. It also achieved a higher Spatial Dissimilarity Index between the ISA and bare soil. However, it is limited by bare gray soil and shadows of clouds and hills. SISAI encourages urban dynamics and inter-urban comparison studies owing to its automatic and unsupervised methodology.

Introduction

Impervious surface area (ISA) mapping is crucial for urban and related studies (Lu *et al.* 2011; Van de Voorde *et al.* 2011; Weng 2012), such as urban flood (Sohn *et al.* 2020), groundwater recharge (Ghimire *et al.* 2021), urban heat island (Yuan and Bauer 2007), environmental studies (Arnold Jr and Gibbons 1996; Chithra *et al.* 2015), climate studies (Bierwagen *et al.* 2010), hydrological studies (Brabec *et al.* 2002; Shao *et al.* 2020; Shuster *et al.* 2005), and land use land cover classification (Lu and Weng 2006). ISA can be natural or manmade. Slonecker *et al.* (2001) defined impervious surfaces as materials that prevent water infiltration into soil. This definition encompasses all types of impervious surface. Jennings *et al.* (2004), on the other hand, defined anthropogenic or artificial impervious surfaces as roads, rooftops, parking lots, driveways, sidewalks, etc.

Spectral index-based urban mapping approaches can include the use of index-based built-up index (IBI) (Xu 2008), the improved normalized difference of built-up index (He *et al.* 2010), vegetation index built-up index (Stathakis *et al.* 2012), built-up area extraction method (BAEM) (Bhatti and Tripathi 2014), ratio normalized difference soil index (RNDSI) (Deng *et al.* 2015), normalized urban areas composite index (NUACI) (Liu *et al.* 2015), combinational built-up index (CBI) (Sun *et al.* 2016), combinational biophysical composition index (Zhang *et al.* 2018), enhanced normalized difference impervious surface index (ENDISI) (Chen *et al.* 2019a), nighttime lights adjusted impervious surface index (NAISI) (Chen *et al.* 2019b), and binary built-up index (BBI) (Zhou *et al.* 2014).

Earlier indices worked well for comparing urban areas with similar geography but were not tested for ISA with diverse geography. Nighttime lights can overcome this limitation, but they are not accurate for predicting ISA and lack spatial resolution (Ch *et al.* 2021; Duque *et al.* 2019). These are still useful in ISA studies.

One of the common problems with mapping ISA is mixed pixel problems, especially with bare soil, owing to their spectral similarity (Deng *et al.* 2019; Lu and Weng 2004). Compared to the ISA, the spectral signatures of bare soil fluctuate phenologically more in infrared regions (near infrared, shortwave infrared (SWIR)1, and SWIR2), particularly in summer (Wang and Li 2019). Some bare soil studies have also used temporal information to minimize bare soil signatures (Chen *et al.* 2004; Mzid *et al.* 2021).

Earlier urban indices were used to map built-up and bare soil areas together. Such indices are the enhanced built-up and bareness index (EBBI) and BBI. Previous spectral indices extracted urban ISA and bare soil area together, such as the EBBI (As-syakur *et al.* 2012) and BBI (Zhou *et al.* 2014). The biophysical composition index (BCI) is a significant attempt to address this problem and uses a tasseled cap transformation to minimize the bare soil signature from the ISA (Deng and Wu 2012). Other indices have been developed to address the mixed pixel problem, such as the RNDSI (Deng *et al.* 2015), modified normalized difference soil index, and normalized ratio urban index (Piyoosh and Ghosh 2017).

Some urban indices are sensitive to waterbodies. The Water Eraser-Normalized Difference Built-Up Index (WE-NDBI) was developed to exclude water areas (Bai *et al.* 2020). Many urban indexing studies have removed water bodies during preprocessing (Deng and Wu 2012). Except for water, the three main Land Use/Land Cover (LULC) elements are vegetation, impervious surfaces, and soil, which were popularized as the vegetation-impervious surface-soil (V-I-S) model by Ridd (1995). Using the V-I-S model, vegetation and bare soil areas were removed to extract impervious surfaces. These include the BCI (Deng and Wu 2012).

However, water indices are sometimes used to enhance the urban indices. For example, NDWI (McFeeters 2007) adds urban features to CBI (Sun *et al.* 2016). In addition, IBI, ENDISI, modified normalized difference impervious surface index (Sun *et al.* 2017), and BAEM are examples of the Modified Normalized Difference Water Index (MNDWI). The MNDWI is also sensitive to ISA after the water area (Xu 2010).

Bai *et al.* (2020) developed a different approach. This study proposed a WE-NDBI by excluding water areas (Bai *et al.* 2020). WE-NDBI significantly increased the urban mapping accuracy to a greater extent than BBI. Many urban indexing studies have removed water bodies during preprocessing (Deng and Wu 2012). Except for water, the three main LULC elements are vegetation, impervious surfaces, and soil, which were popularized as the V-I-S model by Ridd (1995). Zhang *et al.* (2021) proposed the Water-Impervious-Pervious (W-I-P) model, where feature spaces are used to develop an urban composition

Akib Javed, Zhenfeng Shao, Muhammad Nasar Ahmad, Nayyer Saleem, and Fazlul Karim are with the State Key Laboratory of Information Engineering in Surveying, Mapping and Remote Sensing, Wuhan University, Wuhan, Hubei 43007, China (shaozhenfeng@whu.edu.cn; mnassarahmad@gmail.com; nayyersaleem07@gmail.com; f.karim7631@yahoo.com).

Iffat Ara is with Department of Geography and Environment, Islamic University, Kushtia 7003, Bangladesh (iffatru@yahoo.com).

Md. Enamul Huq is with School of Management, Yulin University, Yulin 719000, China and Department of Development Studies, Daffodil International University, Dhaka, Bangladesh. (enamulhuq@yulinu.edu.cn).

Corresponding author: Akib Javed (akibjaved@outlook.com)

Contributed by Tolga Bakirman, June 10, 2023 (sent for review August 16, 2023; reviewed by Nebiye Musaoglu, Alper Yilmaz).

Photogrammetric Engineering & Remote Sensing
Vol. 90, No. 1, January 2024, pp. 33–43.
0099-1112/22/33–43

doi: 10.14358/PERS.23-00043R2

index (UCI). In the W-I-P model, water, impervious surfaces, and pervious surfaces can be derived from a single composition index named UCI.

Traditionally, LULC classification studies have used a single remote sensing (RS) scene manually selected by the researcher to minimize cloud coverage. Cloud-free RS scene selection, sample selection, and land use verification processes are time-consuming and can introduce researcher bias when manually performed. Defining urban boundaries through image classification is challenging (MacGregor-Fors 2011; Xu *et al.* 2021). The delineation of urban ISA from different geographical backgrounds requires common parameters.

Spectral–index-based unsupervised methods are quicker than supervised methods for ISA mapping. This minimizes researcher bias in multi-urban studies. In addition to ISA, urban dynamic measurement requires spatial and temporal dimensions. Spatial and temporal data compatibility is crucial for creating a geographically robust ISA mapping method.

This study proposes a soil-suppressed impervious surface area index (SISAI) using common Landsat bands for composite index mapping, based on annual image stacks and temporal statistics. The aim is to enhance ISA mapping while minimizing bare soil signatures using temporal spectral data. A layer of annual image stacks is used for each city. Atmospheric correction and water removal were performed automatically. Bare soils are addressed in two ways: removing very bright areas across the year and minimizing fluctuating areas by taking the minimum composite of a purpose-built index. This was combined with a soil-free water index to use its ISA sensitivity. SISAI offers a spatially versatile approach to mapping urban ISA across diverse geographies using Landsat's temporal capabilities and spectral statistics.

Materials and Methods

In this study, Landsat was selected as the data set for analysis because of its global coverage and long history. The proposed index uses the most common spectral bands found in Landsat imagery and data from other multispectral sensors. However, the newly developed index SISAI uses only five primary visible and infrared bands: green, red, near-infrared, short-wave infrared 1, and short-wave infrared 2.

Study Area

For this study, the top 12 megacities, globally ranked by population size, were selected to demonstrate and validate the proposed index. A map of the study area was created to show the locations of these megacities in Figure 1.

The megacities in this study had diverse geographical backgrounds. Half of the cities have more water areas, while others, such as Cairo and Karachi, are surrounded by bare soil areas. Two-thirds of the study areas are hilly, showing that the proposed index works across different terrains, with some limitations in hilly regions. To manage the large data sets for all study areas, this study leveraged the Google Earth Engine (GEE) cloud computing platform.

Google Earth Engine

GEE is a popular cloud platform (Gorelick *et al.* 2017) that provides the computational power and large-scale data management required for this temporal study by using historical Landsat data. The full methodology was scripted within GEE for reproducibility, with the code provided in Appendix A.

Study Design

Data Sets and Cloud Removals

Landsat was used for its long archive enabling urban dynamics analysis. Annual *Landsat 8* Level 2 surface reflectance images from 1 January to 31 December of 2021 were used rather than a single image. Landsat quality bands and bit-masks enabled atmospheric correction and reflectance normalization. Clouds, shadows, and snow were removed via bit-masks. 10–100 annual *Landsat 8* images per city generated composites using various index statistics.

Water Masking

The urban ISA indices were adjusted to exclude water signatures by removing water-covered areas (Deng and Wu 2012). A composite water-free index was developed using the median of MNDWI (Xu 2007) and deeply clear waterbody delineation index (DCWDI) (Yue and Liu 2019) to accurately mask water bodies. The median composition mitigated seasonal water variations. Thresholds of 0 and 0.05 were applied to the median MNDWI and DCWDI, respectively, to extract

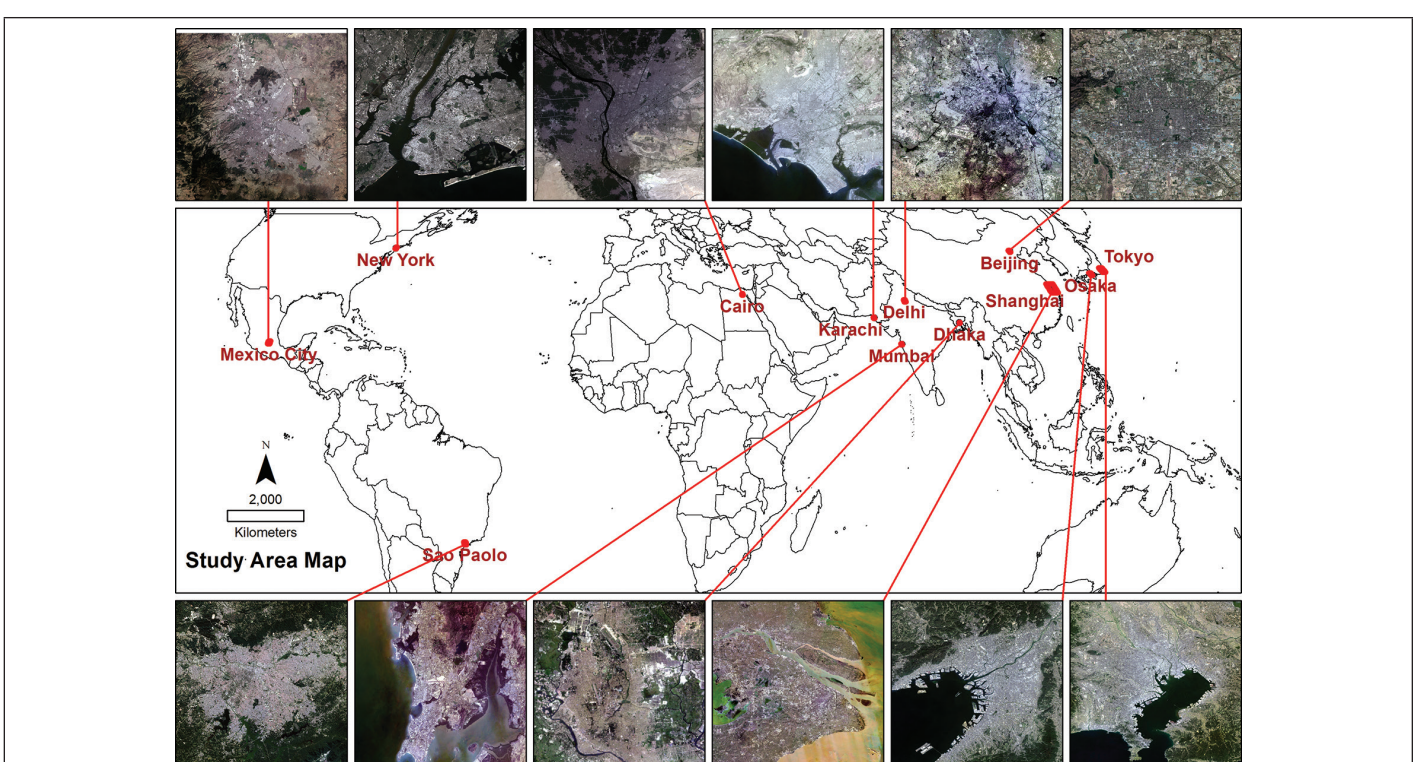

Figure 1. These megacities include Tokyo and Osaka in Japan, Delhi and Mumbai in India, Shanghai and Beijing in China, Sao Paolo in Brazil, Mexico City in Mexico, Dhaka in Bangladesh, Cairo in Egypt, New York in the USA, and Karachi in Pakistan.

water. The resulting composite water-free area (CWFA) is a binary image with 0 for water and 1 for non-water areas.

$$\text{MNDWI} = \frac{\text{Green} - \text{SWIR1}}{\text{Green} + \text{SWIR1}} \quad (1)$$

$$\text{DCWDI} = \sqrt{(\text{Red}^2 + \text{NIR}^2)} \quad (2)$$

$$\text{CWFA} = (\text{median}\text{MNDWI}_T + \text{median}\text{DCWDI}_T) < 1 \quad (3)$$

Here, subset "*T*" refers to the threshold images. CWFA is a binary image of 1 and 0, where "0" is for water, and "1" is for non-water areas.

Development of Composite ISA Index

The study starts with the basic urban indices NDBI (Zha *et al.* 2003), urban index (UI) (Kawamura *et al.* 1997), and a modified version of normalized difference tillage index (NDTI) (Eskandari *et al.* 2016; Van Deventer *et al.* 1997). It is named the Modified Bare and Built-up Index (MBBI). All three indices are based on infrared bands. This study used a simpler version of the UI, the Normalized Difference Urban Index (NDUI). The minimum composition of all the three indices from the annual image composition was adopted to reduce the bare soil signature. A composite ISA index (CISAI) was developed by adding one to each of the three minimum composite urban indices and multiplying them with the CWFA.

$$\text{NDBI} = \frac{\text{SWIR1} - \text{NIR}}{\text{SWIR1} + \text{NIR}} \quad (4)$$

$$\text{NDUI} = \frac{\text{SWIR2} - \text{NIR}}{\text{SWIR2} + \text{NIR}} \quad (5)$$

$$\text{MBBI} = \frac{\text{SWIR2} - \text{SWIR1}}{\text{SWIR2} + \text{SWIR1}} \quad (6)$$

$$\text{CISAI} = (\text{minNDBI} + 1) * (\text{minNDUI} + 1) * (\text{minMBBI} + 1) * \text{CWFA} \quad (7)$$

Here, minNDBI, minNDUI, and minMBBI refer to the minimum annual composite of each index. CISAI is a water-free composite of all the spectral differences of the ISA from the pervious surface areas. The CISAI uses a combination of traditional urban indices such as NDBI, UI, and MBBI. It works well for delineating some cities, but fails to map them, especially those surrounded by low vegetation and high bare soil areas.

Development of terraMNDWI

MNDWI enhances the ISA after water bodies as a second-sensitive LULC class. The study added a minimum composition of MNDWI (minMNDWI) to determine the bare soil areas as a positive value and multiplied it with CWFA to obtain terraMNDWI. The function of terraMNDWI is to increase the separability of the bare soil and ISA.

$$\text{terraMNDWI} = (\text{minMNDWI} + 1) * \text{CWFA} \quad (8)$$

Development of Short-Wave Infrared Soil Index

A simple yet effective soil index, Short-Wave Infrared Soil Index (swirSoil), was proposed to map bright sandy areas, such as deserts and beaches. The swirSoil index is a quadruple product of two Landsat SWIR bands. The purpose of swirSoil is to remove bright soil areas from remote sensing images (RSI), such as desert and beach areas.

$$\text{swirSoil} = \text{SWIR1} * \text{SWIR2} * 4 \quad (9)$$

Development of the Soil-Suppressed ISA Index

SISAI takes advantage of CISAI, terraMNDWI, and swirSoil indices to suppress the similarity between ISA and bare soil. The SISAI was calculated by subtracting the swirSoil from the product of the CISAI and terraMNDWI.

$$\text{SISAI} = (\text{CISAI} * \text{terraMNDWI}) - \text{swirSoil} \quad (10)$$

The entire method is shown in Figure 2.

The complete methodology is shown in Figure 2. In the next section, the spectral difference index (SDI) was designed to test the performance of the indices.

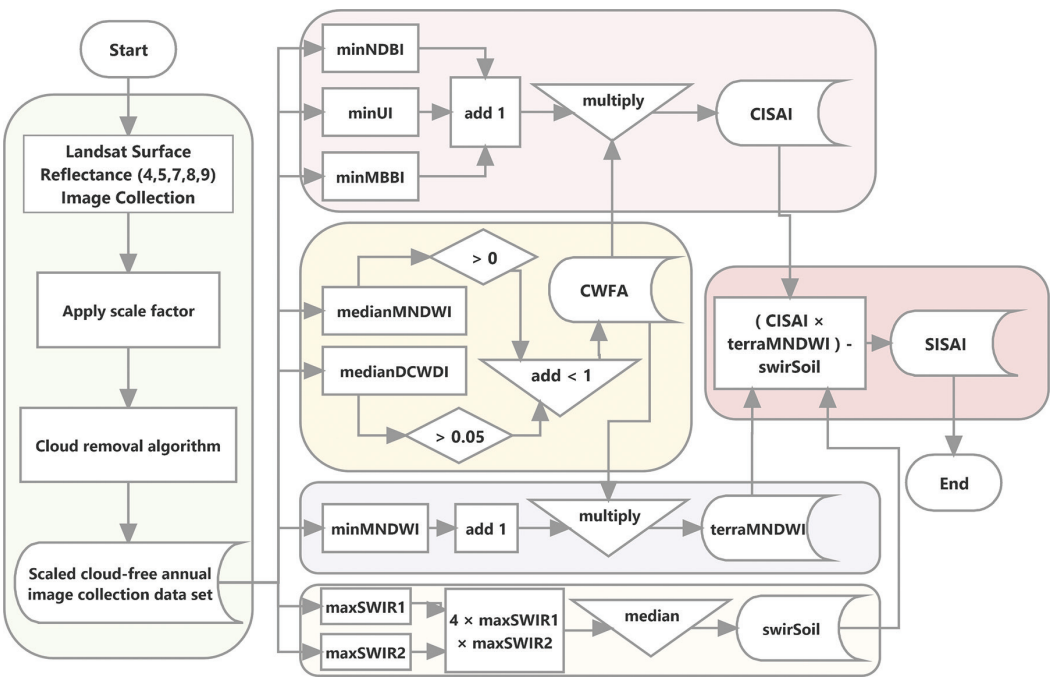

Figure 2. Complete methodology of SISAI. Here, CWFA means composite water-free area; CISAI means composite ISA index; SISAI means soil-suppressed ISA index. DCWDI = deeply clear waterbody delineation index; MBBI = Modified Bare and Built-up Index; NDBI = normalized difference built-up index; UI = urban index; MNDWI = Modified Normalized Difference Water Index; SWIR = shortwave infrared.

Calculation of Spectral Difference Index

The SDI was used to evaluate the strength of each index in classifying urban ISA and other major LULC classes (Bouhennache *et al.* 2019; Kaufman and Remer 1994). SDI uses the mean and standard deviation indices of each class to determine the distinguishability of the two LULC image classes. The LULC patches for each class were digitized using Google Earth images as reference maps. The SDI formula is as follows:

$$\mathrm{SDI} = \left| \frac{\overline{\mu_1} - \overline{\mu_2}}{\overline{\sigma_1} + \overline{\sigma_2}} \right| \tag{11}$$

where μ and σ represent the mean value and standard deviation of the LULC image classes, respectively, and subscripts "1" and "2" represent the first and second LULC image classes, respectively. This study compared the UCI, CISAI, and SISAI using the SDI. Sample areas for ISA, water, vegetation, and bare soil were taken separately for each city using Google Earth images with *Landsat 8* red/green/blue (RGB) true color composition for sampling.

Optimal Threshold Value

The study tested a range of thresholds from 0.02 to 0.18 to determine the optimal threshold value for spatial comparison studies among urban areas. The initial search found that overall accuracy peaked between 0.1 to 0.12 with an interval of 0.01. A refined search with an interval of 0.001 revealed that a threshold of 0.103 achieved the highest accuracy assessment results for the four selected city areas. This optimal threshold value provided the lowest combined omission and commission errors as well as the highest F1 score. Therefore, this study determined that 0.103 is the optimal threshold value for spatial comparison studies among urban areas.

Quality Assessment

Random Sampling Points

The sampling area was manually chosen from the study areas, including urban, peri-urban, and non-urban areas (Figure 3). For validation, 7200 stratified random sampling points were selected across the study area, with 600 sampling points taken per city. The sampling points were derived using ArcToolbox from ArcGIS (ArcToolbox\Data Management Tools\Sampling\Create Random Points).

Ground Truth of Reference Points

The reference points were checked using the latest Google Earth Pro images at a higher spatial resolution. Reference data were collected in the last week of May 2022. For all 12 cities, Google Earth images were updated in 2021 and had a ground spatial resolution of 1 – 10 m.

Classified Urban ISA

The study exported SISAI images using GEE. The newly classified urban ISA areas created for each study were from SISAI images, and the optimal threshold value was 0.103, resulting in binary images with "1" being ISA and "0" being water or the pervious area. This classification can be done using the "reclassify" tool from ArcToolbox (ArcToolbox\spatial analyst tools\reclass\reclassify) or using the "export.image.toDrive" function from GEE.

Extraction of Classified Points Value

The classified urban ISA binary images and random sampling points were used to extract the respective SISAI values for the validation study. The "Extract Values to Points" tool from ArcToolbox of ArcGIS (ArcToolbox\Spatial Analyst Tools\Extraction\Extract by Points) was used to extract classified points.

Accuracy Assessment Metrics

This study used only two classes: ISA and other areas. Therefore, a confusion matrix was used to determine whether the classified points were ISA. The binary confusion matrix, shown in Table 1, is useful for studies with only two classes. The binary confusion matrix shows the accuracy assessment equations (Table 1).

Table 1. Binary confusion matrix.

	Classified: No	Classified: Yes
Reference: No	True Negative (TN)	False Positive (FP)
Reference: Yes	False Negative (FN)	True Positive (TP)

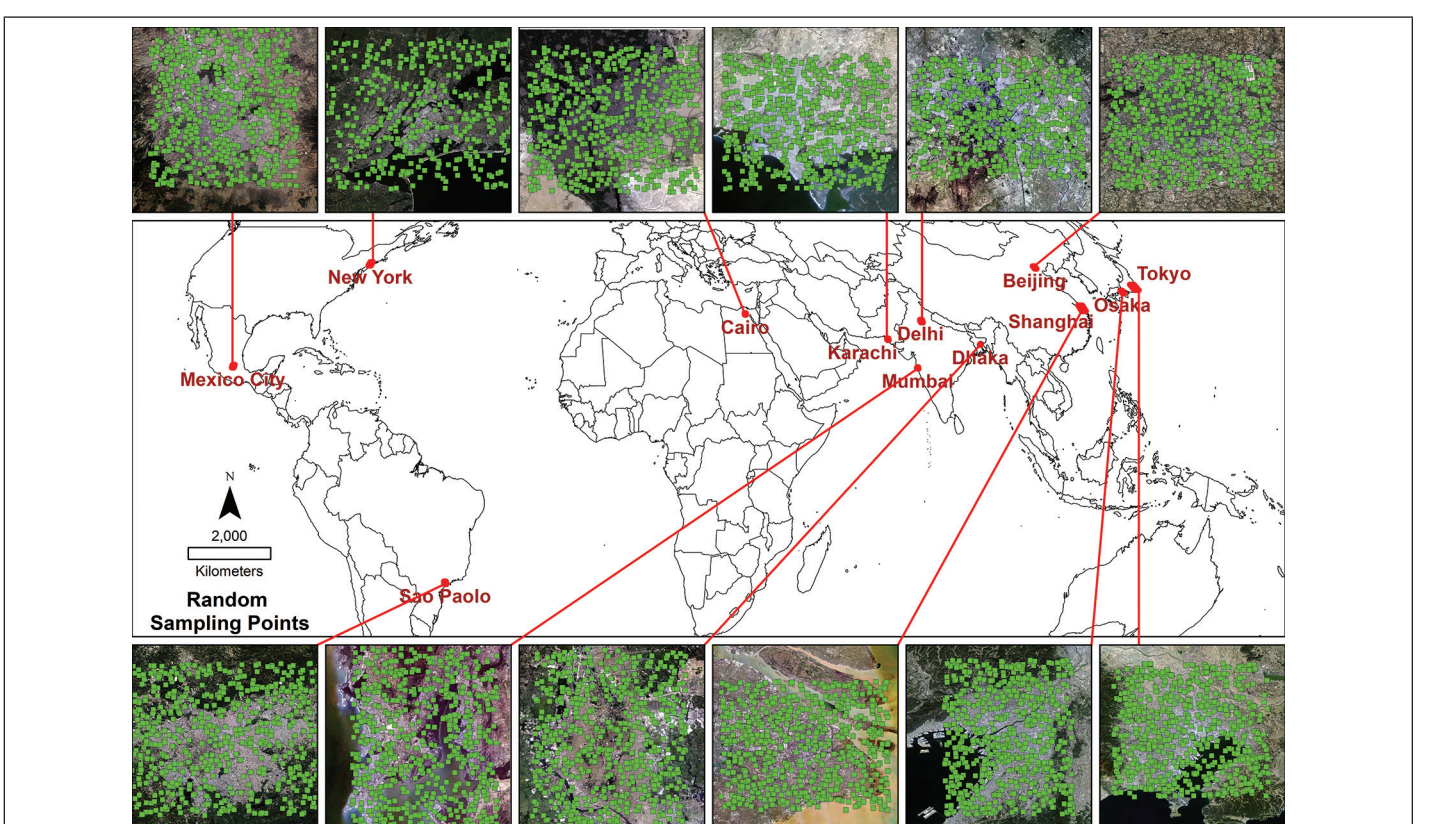

Figure 3. Random sampling points for all 12 megacities.

The accuracy assessment metrics used in this study were producer accuracy, user accuracy, overall accuracy (Story and Congalton 1986), and the F1 score (Chicco and Jurman 2020). Accuracy assessment equations (Equations12–17) were formulated to deal with only two classes (Chicco *et al.* 2021). All the equations are described below (Equations12–17).

$$\text{Overal Accuracy (OA)} = (TP + TN)/(TN + FP + FN + TP) \quad (12)$$

$$\text{Sensitivity} = TP/(TP + FN) \quad (13)$$

$$\text{Omission error} = FN/(FN + TP) \quad (14)$$

$$\text{Comission error} = FP/(FP + TP) \quad (15)$$

$$\text{F1 score} = \frac{2 * TP}{2 * TP + FP + FN} \quad (16)$$

where OA = Overall Accuracy, TP = True Positive, TN = True Negative, FP = False Positive, and FN = False Negative. The accuracy assessment comparison table shows the combined results and city-wise standard deviation (SD) for all study areas. To calculate the SD from the samples, the following formula was used:

$$SD = \sqrt{\frac{1}{N-1}\sum_{i=1}^{N}(x_i - \bar{x})^2} \quad (17)$$

where the denominator $N - 1$ is used because the calculation is based on sample data rather than population data.

Results

This section presents the results of several evaluations and assessments related to the effectiveness of the various indices and methods. First, it reports on the evaluation of the UCI, CISAI, and SISAI using an SDI-based index. Second, it discusses the enhancement of ISA with SISAI. Third, it describes a threshold-based approach for ISA extraction using SISAI. Finally, it provides an accuracy assessment for the SISAI across 12 different cities. Through these evaluations and assessments, this section aims to gain insights into the effectiveness and applicability of these methods in different contexts.

Spectral Difference Index for UCI, CISAI, and SISAI

SISAI showed better separability between the LULC classes of ISA and bare soil. This improved SDI performance was observed in every study city. CISAI showed higher SDI values for the ISA and water classes. There were no fixed patterns in ISA or vegetation classes. Below are the SDI values of UCI, CISAI, and SISAI for the study areas.

Table 2 shows that for all megacities, except for Shanghai, SISAI had the highest SDI values compared to UCI and CISAI. Higher SDI values represent better separability between ISA and bare soil. SISAI performs better than the other indices in separating the ISA from bare soil.

Enhancement of ISA with SISAI

The CISAI improves traditional single-index mapping by significantly reducing soil signatures (Figure 4b, Cairo and Karachi). Desert cities such as Cairo are delineated, while urban fringes in cities such as Beijing are less distinct. Hilly urban areas are differentiated from bare hills, as is the case in Karachi. Compared to SISAI, CISAI better separates ISA from bare soils, including bare hills, mountains, river islands, sand-filled wetlands, and deserts. (Figure 4a and 4b). Traditional indices cannot sufficiently distinguish ISA from bare soil.

Extract ISA with SISAI

This study uses a common threshold value of 0.103 for all 12 cities (Figure 4a and 4b), showing that SISAI can map megacities globally using 30m *Landsat 8* and performs well. A threshold of 0.1 worked generally based on trial and error, then refined to 0.103 using Tokyo, Beijing, Cairo, and Mexico City. Thus SISAI is an urban index like NUACI (Liu *et al.* 2015; Liu *et al.* 2018) and UCI (Zhang *et al.* 2021), using only *Landsat 8* unlike additional data sets. The multispectral bands were from the previous Landsat, enabling historical analysis. Using additional data sets, such as NTL data sets, can significantly improve the accuracy of results in regional-scale applications.

The spectral confusion between the ISA and bare soil was addressed in two ways. Primarily, the minimum composite of annual urban indices reduced bare soil signatures, particularly in fluctuating or vegetated areas. Second, the water-free minimum MNDWI composite was multiplied by the ISA composite, leveraging the ISA sensitivity and soil differentiation of MNDWI. For water masking, median composites of MNDWI and DCWDI were used for stable water mapping. These indices minimize phenological effects. Landsat quality bands reduce cloud shadows, although building shadows may be included from minimum compositing. Importantly, this unsupervised method uses GEE cloud and public Landsat data for robust and rapid reproducibility. The results are shown with true color, CISAI, SISAI, and extracted urban ISA.

Table 2. SDI values of UCI, CISAI, and SISAI for ISA with bare soil, water, and vegetation LULC classes. The cells highlighted in green showed the highest performance compared to the other two indices.

	ISA & Bare Soil			ISA & Water			ISA & Vegetation		
Megacities	UCI	CISAI	SISAI	UCI	CISAI	SISAI	UCI	CISAI	SISAI
Tokyo	0.88	0.15	0.96	1.80	3.55	3.14	3.76	2.76	2.80
Delhi	1.24	0.94	2.49	3.27	8.27	6.05	2.91	5.99	5.37
Shanghai	0.75	1.64	1.02	2.97	4.28	1.83	3.38	2.97	1.59
Sao Paolo	0.09	0.37	0.94	2.10	5.73	3.22	4.56	4.77	2.91
Mexico	2.00	2.32	2.93	2.48	6.51	3.98	5.52	4.62	3.47
Dhaka	0.17	1.22	2.25	2.74	7.97	7.23	2.86	6.35	6.60
Cairo	0.74	0.08	1.32	0.40	7.72	3.65	3.94	4.55	2.91
Beijing	1.38	1.79	2.31	1.65	2.92	2.36	1.28	2.08	1.86
Mumbai	0.91	1.18	1.21	3.42	3.96	2.54	1.44	2.23	1.41
Osaka	1.09	0.70	1.36	0.50	4.40	4.48	4.09	3.66	4.04
New York	0.72	0.27	1.14	0.07	5.56	3.22	2.22	4.62	3.07
Karachi	1.10	0.02	1.28	2.58	11.81	7.01	4.73	9.39	6.19

CISAI = composite ISA index; ISA = impervious surface area; LULC = Land Use/Land Cover; SISAI = Soil-Suppressed Impervious Surface Area Index; UCI = urban composition index.

Quantitative Accuracy Assessment

The accuracy assessment in Table 3 shows the overall accuracy, omission error, commission error, and F1 score of the SISAI for all megacities. It is important to understand Table 3 that the higher the value for overall accuracy and the F1 score, the better. The lower the value for the omission and commission errors, the better.

Table 3 shows that Osaka, Japan had the highest overall accuracy. Osaka also showed good performance in other accuracy metrics, such as commission errors and F1 scores. This is mainly because, on a

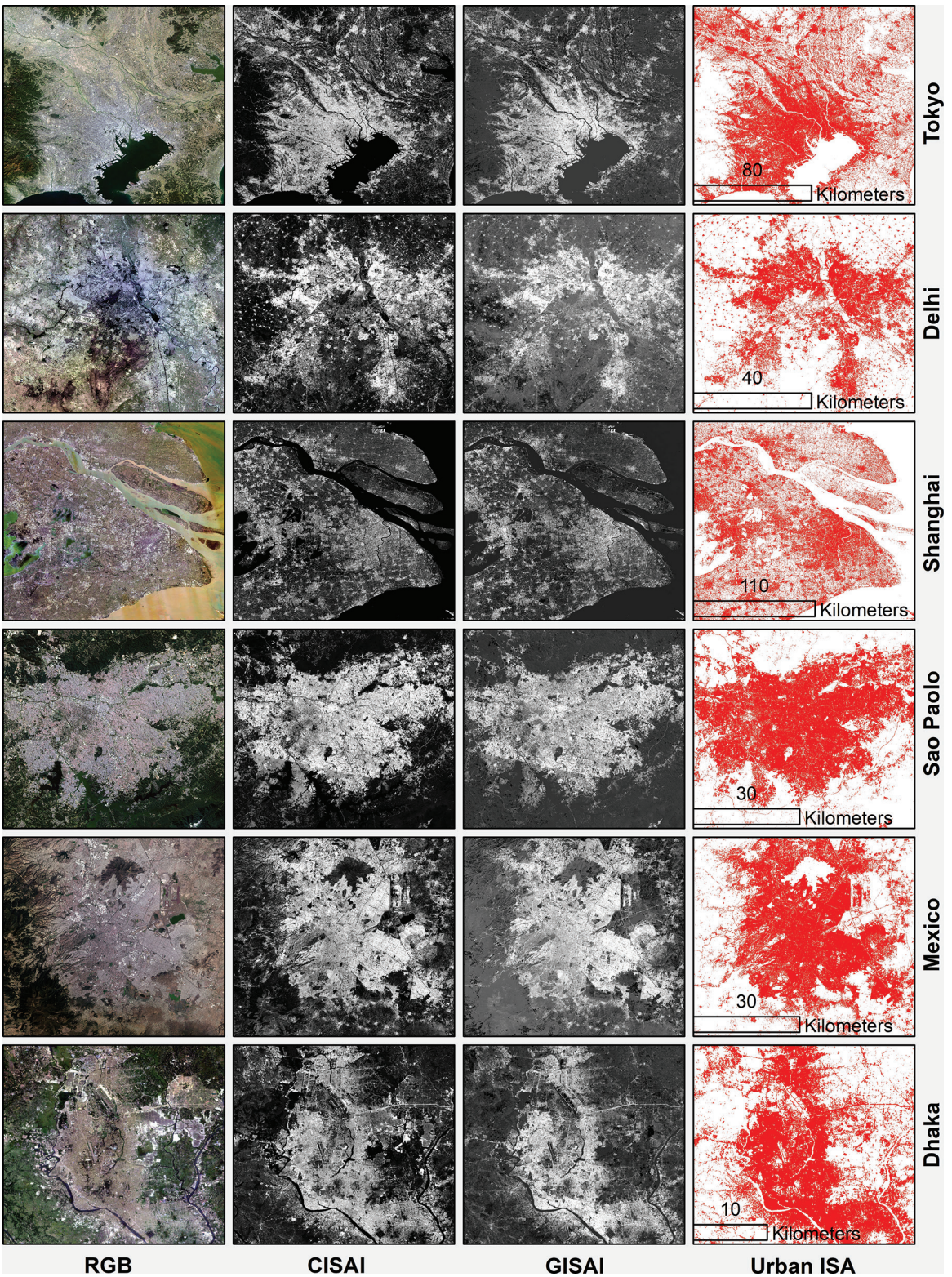

Figure 4. (a) (from left to right) Red/green/blue (RGB) true color composition, composite ISA index (CISAI), Soil-Suppressed Impervious Surface Area Index (SISAI), and SISAI-based urban impervious surface area (ISA) mapping using a threshold of 0.103. The first six megacities (from top to bottom) are: 1. Tokyo, 2. Delhi, 3. Shanghai, 4. Sao Paolo, 5. Mexico City, 6. Dhaka (continued).

percentage-wise basis, Osaka has a very low proportion of bare soil. By contrast, Dhaka had the lowest overall accuracy and commission errors. However, Dhaka also had the least omission errors. New York had the poorest omission errors and F1 scores.

The result section shows the SDI performance table comparing the ISA class with bare soil, water bodies, and vegetation for UCI, CISAI, and SISAI. Table 3 shows the higher performance of SISAI in separating ISA from bare soil. Later, it described how SISAI enhances ISA signatures and how a single threshold extracts ISA areas from the

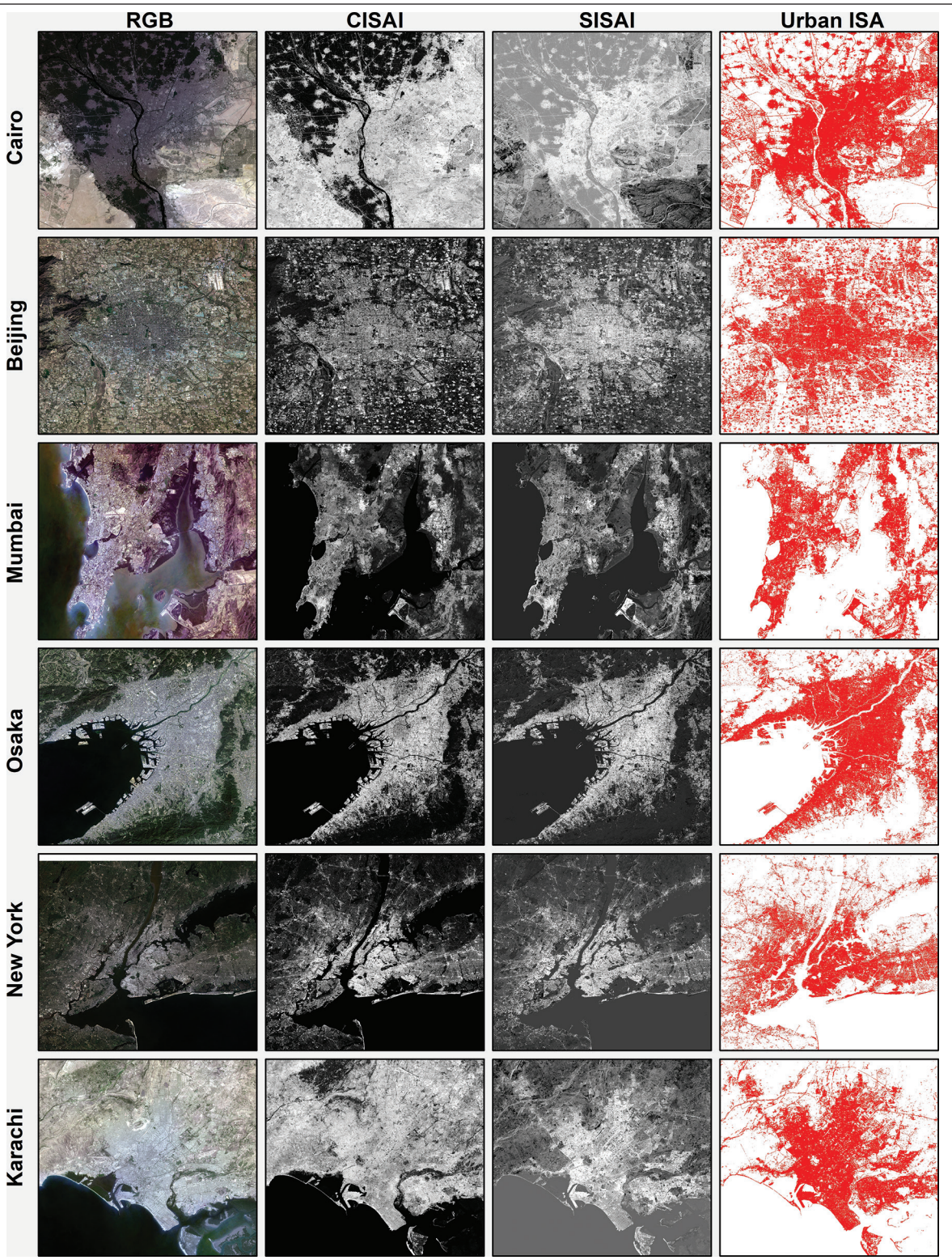

Figure 4. (b) (continued from Figure 4a) The last six megacities are (from top to bottom): 7. Cairo, 8. Beijing, 9. Mumbai, 10. Osaka, 11. New York, and 12. Karachi. CISAI = composite ISA index; ISA = impervious surface area; RGB = red/green/blue; Soil-Suppressed Impervious Surface Area Index (SISAI).

Table 3. Quantitative accuracy assessment of the Soil-Suppressed Impervious Surface Area Index (SISAI) for the top 12 megacities. The Green highlighted color indicates the highest accuracy, and the red highlighted color indicates the lowest accuracy.

Megacity	Overall Accuracy	Omission Error	Commission Error	F1 Score
Tokyo	0.898	0.060	0.164	0.885
Delhi	0.862	0.139	0.204	0.827
Shanghai	0.848	0.146	0.348	0.739
Sao Paolo	0.912	0.099	0.134	0.883
Mexico City	0.895	0.089	0.122	0.894
Dhaka	0.773	0.041	0.378	0.755
Cairo	0.877	0.105	0.140	0.877
Beijing	0.885	0.130	0.098	0.886
Mumbai	0.868	0.137	0.256	0.799
Osaka	0.938	0.081	0.051	0.934
New York	0.870	0.323	0.201	0.733
Karachi	0.867	0.134	0.214	0.824

background. This demonstrates the indexing capability of CISAI and SISAI with Landsat RSI. This showed how the threshold extracted the SISAI-based urban ISA capable of urban area mapping with RGB maps per city. The section ends with an accuracy assessment table for the SISAI per city. section, the significance of the methodology and findings are discussed.

Discussion

The SISAI methodology and its findings are important for several reasons. The SDI values were higher for the ISA and bare soil classes. Second, the SISAI can compare multiple cities from diverse geographical backgrounds. Third, the variability of thresholds can affect the accuracy of the ISA classification and has the potential to be a global urban mapping index.

Significance of the Study

SISAI is a new urban mapping index developed to effectively distinguish between bare soil and ISA in cities surrounded by bare soil land cover. It combines three existing indices and several composite indices, including the CWFA, water-free MNDWI (terraMNDWI), and a novel composite soil index (swirSoil). These composites help remove water pixels, enhance separability between bare soil and urban ISA, and suppress the bare soil signature.

SISAI has been performed in cities such as Cairo and Delhi, demonstrating its effectiveness in mapping urban areas even in challenging environments. SISAI's limited band requirements of SISAI make it suitable for long-term Landsat analyses, and its unsupervised nature ensures fast application and unbiased results. However, it struggles with bare grey soil areas that do not change the reflectance seasonally. This limitation can potentially be addressed using nighttime light data sets, such as NUACI (Liu *et al.* 2015) and NAISI (Chen *et al.* 2019b). Overall, SISAI is a promising index for urban mapping and comparative studies across various geographical backgrounds.

SDI Comparison of UCI, CISAI, and SISAI

CISAI distinguishes ISA from water and vegetation, but not from bare soil. Thus, CISAI can map water-free ISA where bare soil is negligible, while SISAI is better with significant bare soil. For inter-urban studies, even one urban area with bare soil makes the SISAI more suitable.

The SISAI values indicate a higher ISA proportion, while the CISAI values show a higher ISA or bare soil. The UCI uses two thresholds for ISA versus other land classes, so higher UCI values do not necessarily mean more ISA. The median annual images used here differ from the single image for UCI, potentially affecting the poorer UCI performance in SDI, particularly for ISA and bare soil.

For stratified sampling, the physical characteristics of the study area are critical. The ISA, bare soil, water, and vegetation spectral characteristics vary across cities, possibly explaining the SDI underperformance in some cities, such as Beijing and Mumbai, with low vegetation. Attempts were made for representative vegetation sampling, but a lower vegetation SDI was observed in these cities. However, water and vegetation indices can minimize these weaknesses. The key contribution of SISAI is improved ISA and bare soil SDI over UCI and CISAI, although SISAI performed poorly in Shanghai.

Comparison with Similar Studies

The NUACI2015 mainly depends on the annual maximum vegetation composite index (Liu *et al.* 2015). Urban areas typically cover small portions of land, which act as anomalies and are surrounded by vegetation. Thus, vegetation composites alone can be used to map urban areas within dominant vegetation. However, NUACI failed without dominant background vegetation. The SISAI works in both humid and arid areas. The 2018 NUACI variant (NUACI2018) (Liu *et al.* 2018) uses three normalized indices: NDWI, NDVI (Chen and Cihlar 1996), and NDBI. NUACI2018-based urban classification requires sampling diverse urban areas for calibration, unlike the sampling-independent SISAI method, which uses only accuracy measurements. This accelerates the SISAI urban ISA measurements. Both NUACI versions used nighttime light data, easily incorporated in SISAI as additional layers, potentially enabling global SISAI urban mapping. The SISAI is well suited for urban and peri-urban areas. Importantly, the SISAI relies solely on Landsat multispectral data for more authentic ISA mapping, which is applicable across ISA studies and enable temporal studies with future prediction (Ahmad *et al.* 2023).

Figure 5 compares the RGB, Global Human Settlement Layer (GHSL) (2014), World Settlement Footprint (WSF) (2015), GAIA (2018), UCI (2021), and SISAI (2021). SISAI is similar to the supervised GHSL, WSF, and GAIA maps. The UCI differs, with fewer ISA pixels in each city except Karachi, where oceans appear urban owing to clouds. The UCI also has low accuracy in Mexico City, with a sparse ISA. UCI uses single cloud-free images (Zhang *et al.* 2021), while this study took annual medians of image collections. However, medians may retain clouds, potentially affecting the UCI performance. The RGB composites showed minimal clouds and the UCI had poor accuracy (Table 4).

Table 4. Quantitative accuracy assessment of the urban composition index (UCI) and Soil-Suppressed Impervious Surface Area Index (SISAI) for the top 12 megacities. The bold formatted values indicate that SISAI performs lower than UCI.

	Overall Accuracy		Omission Error		Commission Error		F1 Score	
Megacity	UCI	SISAI	UCI	SISAI	UCI	SISAI	UCI	SISAI
Tokyo	0.835	0.898	0.330	0.060	**0.031**	**0.164**	0.792	0.885
Delhi	0.808	0.862	0.410	0.139	**0.075**	**0.204**	0.720	0.827
Shanghai	0.778	0.848	0.463	0.146	**0.264**	**0.348**	0.621	0.739
Sao Paolo	0.702	0.912	0.750	0.099	**0.079**	**0.134**	0.393	0.883
Mexico City	0.825	0.895	0.286	0.089	**0.072**	**0.122**	0.807	0.894
Dhaka	0.727	0.773	0.326	0.041	**0.192**	**0.378**	0.735	0.755
Cairo	0.687	0.877	0.515	0.105	0.162	0.140	0.615	0.877
Beijing	0.830	0.885	0.254	0.130	0.104	0.098	0.814	0.886
Mumbai	0.765	0.868	0.531	0.137	**0.219**	**0.256**	0.587	0.799
Osaka	0.905	0.938	0.170	0.081	**0.042**	**0.051**	0.890	0.934
New York	0.868	0.870	0.451	0.323	**0.151**	**0.201**	0.667	0.733
Karachi	0.803	0.867	0.274	0.134	0.229	0.214	0.748	0.824

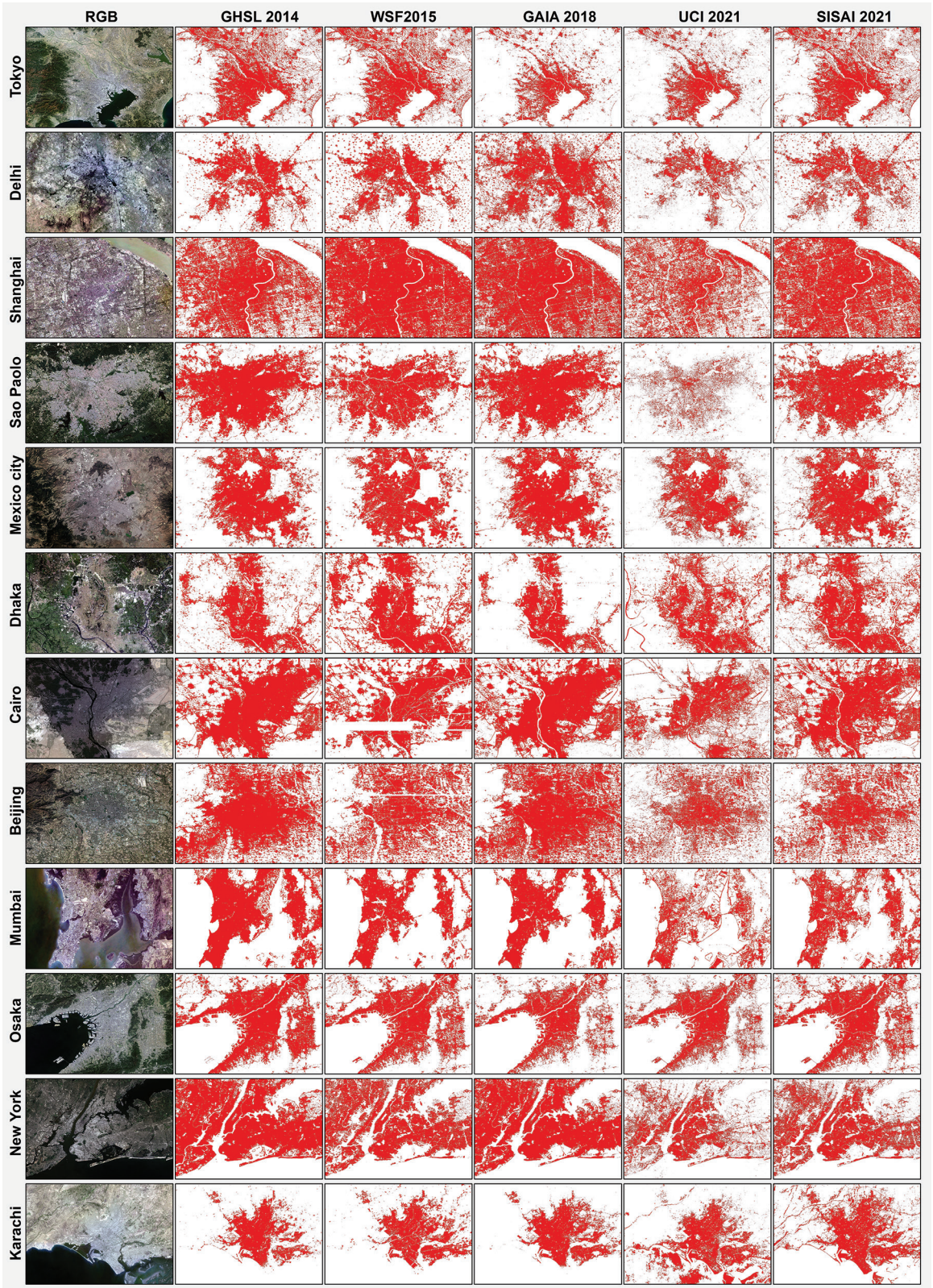

Figure 5. Urban area extraction result comparison between urban composition index (UCI) and Soil-Suppressed Impervious Surface Area Index (SISAI) for Tokyo, Delhi, Shanghai, Sao Paolo, Mexico, Dhaka, Cairo, Beijing, Mumbai, Osaka, New York, and Karachi. GHSL = Global Human Settlement Layer; RGB = red/green/blue; WSF = World Settlement Footprint.

In summary, SISAI performs comparably to recent global supervised ISA products using the same annual median *Landsat 8* composites as the simple unsupervised UCI method but with higher accuracy. The annual median composites minimized the noise while retaining the ISA signals.

Table 4 shows that SISAI has higher accuracy than UCI overall, except for lower commission errors in nine of the 12 cities. However, Zhang *et al.* (2021) reported 0.931 UCI accuracy in Beijing, versus 0.830 here for UCI and 0.885 for SISAI. This study used annual median image composites rather than manual single-image selection, possibly affecting the UCI performance. Random sampling may also affect the accuracy of UCI. Overall, UCI is a good urban index but is limited for bare soil areas, while SISAI performs well across all metrics. The annual medians minimized noise while retaining ISA signals to boost SISAI accuracy over the UCI.

Here, "SD" refers to the standard deviation (SD), which shows consistency across 12 cities. SISAI showed the lowest accuracy in Dhaka and UCI in Cairo, both of which had extensive bare soil. However, the SISAI minimizes the variability in accuracy metrics across cities (Table 4).

Table 5 shows that the SISAI exceeds the UCI accuracy overall, except for commission errors. City-specific threshold optimization could improve single-city studies, but a universal threshold enables easier inter-urban comparisons. Nevertheless, SISAI minimizes intra-urban variability versus UCI and exceeds UCI in combined results across all metrics except commission errors. In conclusion, the SISAI is better suited than the UCI as an urban index for ISA mapping, providing more consistent accuracy across diverse cities.

Table 5. Comparative accuracy assessment of Soil-Suppressed Impervious Surface Area Index (SISAI) and urban composition index (UCI). The green-highlighted color indicates higher accuracy.

Accuracy Assessment	Combined		SD	
	SISAI	UCI	SISAI	UCI
Overall Accuracy	0.874	0.794	0.040	0.066
Omission Error	0.116	0.384	0.071	0.158
Commission Error	0.189	0.133	0.097	0.079
F1 Score	0.846	0.721	0.067	0.133

Variable Thresholds and Accuracy

It is important to know that omission and commission errors are interlinked, and reducing one error with thresholds increases the other. This study aimed to maximize overall accuracy across all cities using a single global threshold of 0.103. Studies on a single city or region can optimize thresholds for higher accuracy. Lowering the threshold reduces the omission error, while increasing it reduces the commission error for the ISA. This study aims to minimize bare soil signatures. Therefore, the threshold continues to increase until the commission error is minimal and by accepting a high ISA omission error. To extract the maximum ISA, the threshold was lowered until the ISA omission error is minimal, accepting a high commission error. To achieve the best classification accuracy, researchers should optimize thresholds to balance omission and commission errors, based on their particular objectives.

Conclusion

The SISAI has been developed to enhance ISA extraction and aid urban studies. It presents improved separability of ISA from bare soil, is applicable across diverse geographic areas, and facilitates longer temporal analysis via historical remote sensing imagery. SISAI uses infrared band indices, excludes water areas, and applies MNDWI and SWIR-based indices to improve ISA extraction. Two novel indices were formulated for SISAI using Landsat SWIR bands: the MBBI and the SWIR weighted soil index (swirSoil). A threshold value of 0.103 was used to identify urban areas in the 12 megacities.

The accuracy assessment revealed higher commission errors than omission errors, suggesting that lowering the threshold value can improve the results. SISAI demonstrated higher spatial accuracy and better overall accuracy, omission errors, and F1 scores than the similar urban index UCI. Furthermore, SISAI provides a more precise annual estimation of the ISA for urban areas, including arid cities such as Cairo and Karachi, as well as coastal and humid cities. However, SISAI's performance of SISAI depends on effective image preprocessing to remove shadows and struggles with permanent bare gray soil. The latter issue can be addressed via the use of nighttime light data. Despite these limitations, SISAI's broad applicability and accuracy of SISAI mark a significant advancement in ISA extraction and urban studies.

Acknowledgments

Conflicts of Interest: The authors declare no conflicts of interest.

Appendix A: GEE Script Repository

The following link is used to access the script used in the study. The user requires a Google Earth Engine account to access it.

https://code.earthengine.google.com/6593ff6eff917975658c0f26f0febd1c

References

Ahmad, M.N., Shao, Z., & Javed, A. (2023). Modelling land use/land cover (LULC) change dynamics, future prospects, and its environmental impacts based on geospatial data models and remote sensing data. *Environ Sci Pollut Res Int, 30*, 32985-33001

Arnold Jr, C.L., & Gibbons, C.J. (1996). Impervious surface coverage: the emergence of a key environmental indicator. *Journal of the American planning Association, 62*, 243-258

As-syakur, A.R., Adnyana, I.W.S., Arthana, I.W., & Nuarsa, I.W. (2012). Enhanced Built-Up and Bareness Index (EBBI) for Mapping Built-Up and Bare Land in an Urban Area. *Remote Sensing, 4*, 2957-2970

Bai, Y., He, G., Wang, G., & Yang, G. (2020). WE-NDBI-A new index for mapping urban built-up areas from GF-1 WFV images. *Remote Sensing Letters, 11*, 407-415

Bhatti, S.S., & Tripathi, N.K. (2014). Built-up area extraction using Landsat 8 OLI imagery. *GIScience remote sensing, 51*, 445-467

Bierwagen, B.G., Theobald, D.M., Pyke, C.R., Choate, A., Groth, P., Thomas, J.V., & Morefield, P. (2010). National housing and impervious surface scenarios for integrated climate impact assessments. *Proc Natl Acad Sci U S A, 107*, 20887-20892

Bouhennache, R., Bouden, T., Taleb-Ahmed, A., & Cheddad, A. (2019). A new spectral index for the extraction of built-up land features from Landsat 8 satellite imagery. *Geocarto International, 34*, 1531-1551

Brabec, E., Schulte, S., & Richards, P.L. (2002). Impervious surfaces and water quality: a review of current literature and its implications for watershed planning. *Journal of planning literature, 16*, 499-514

Ch, R., Martin, D.A., & Vargas, J.F. (2021). Measuring the size and growth of cities using nighttime light. *Journal of Urban Economics, 125*, 103254

Chen, J., Yang, K., Chen, S., Yang, C., Zhang, S., & He, L. (2019a). Enhanced normalized difference index for impervious surface area estimation at the plateau basin scale. *Journal of Applied Remote Sensing, 13*, 19

Chen, J.M., & Cihlar, J. (1996). Retrieving leaf area index of boreal conifer forests using Landsat TM images. *Remote Sensing of Environment, 55*, 153-162

Chen, W., Liu, L., Zhang, C., Wang, J., Wang, J., & Pan, Y. (2004). Monitoring the seasonal bare soil areas in Beijing using multitemporal TM images. In, *IGARSS 2004. 2004 IEEE International Geoscience and Remote Sensing Symposium* (pp. 3379-3382): IEEE

Chen, X., Jia, X., & Pickering, M. (2019b). A Nighttime Lights Adjusted Impervious Surface Index (NAISI) with Integration of Landsat Imagery and Nighttime Lights Data from International Space Station. *International Journal of Applied Earth Observation and Geoinformation, 83*

Chicco, D., & Jurman, G. (2020). The advantages of the Matthews correlation coefficient (MCC) over F1 score and accuracy in binary classification evaluation. *BMC genomics, 21*, 1-13

Chicco, D., Warrens, M.J., & Jurman, G. (2021). The Matthews correlation coefficient (MCC) is more informative than Cohen's Kappa and Brier score in binary classification assessment. *Ieee Access, 9*, 78368-78381

Chithra, S., Nair, M.H., Amarnath, A., & Anjana, N. (2015). Impacts of impervious surfaces on the environment. *International Journal of Engineering Science Invention, 4*, 27-31

Deng, C., & Wu, C. (2012). BCI: A biophysical composition index for remote sensing of urban environments. *Remote Sensing of Environment, 127*, 247-259

Deng, Y., Wu, C., Li, M., & Chen, R. (2015). RNDSI: A ratio normalized difference soil index for remote sensing of urban/suburban environments. *International Journal of Applied Earth Observation and Geoinformation, 39*, 40-48

Deng, Z., Zhu, X., He, Q., & Tang, L. (2019). Land use/land cover classification using time series Landsat 8 images in a heavily urbanized area. *Advances in Space Research, 63*, 2144-2154

Duque, J.C., Lozano-Gracia, N., Patino, J.E., Restrepo, P., & Velasquez, W.A. (2019). Spatiotemporal dynamics of urban growth in Latin American cities: An analysis using nighttime light imagery. *Landscape and Urban Planning, 191*, 103640

Eskandari, I., Navid, H., & Rangzan, K. (2016). Evaluating spectral indices for determining conservation and conventional tillage systems in a vetch-wheat rotation. *International Soil and Water Conservation Research, 4*, 93-98

Ghimire, U., Shrestha, S., Neupane, S., Mohanasundaram, S., & Lorphensri, O. (2021). Climate and land-use change impacts on spatiotemporal variations in groundwater recharge: A case study of the Bangkok Area, Thailand. *Science of the Total Environment, 792*, 148370

Gorelick, N., Hancher, M., Dixon, M., Ilyushchenko, S., Thau, D., & Moore, R. (2017). Google Earth Engine: Planetary-scale geospatial analysis for everyone. *Remote Sensing of Environment, 202*, 18-27

He, C., Shi, P., Xie, D., & Zhao, Y. (2010). Improving the normalized difference built-up index to map urban built-up areas using a semiautomatic segmentation approach. *Remote Sensing Letters, 1*, 213-221

Jennings, D.B., Jarnagin, S.T., & Ebert, D.W. (2004). A modeling approach for estimating watershed impervious surface area from national land cover data 92. *Photogrammetric Engineering and Remote Sensing, 70*, 1295-1307

Kaufman, Y.J., & Remer, L.A. (1994). Detection of forests using mid-IR reflectance: an application for aerosol studies. *Ieee Transactions on Geoscience and Remote Sensing, 32*, 672-683

Kawamura, M., Jayamanna, S., & Tsujiko, Y. (1997). Quantitative evaluation of urbanization in developing countries using satellite data. *Doboku Gakkai Ronbunshu, 1997*, 45-54

Liu, X., Hu, G., Ai, B., Li, X., & Shi, Q. (2015). A Normalized Urban Areas Composite Index (NUACI) Based on Combination of DMSP-OLS and MODIS for Mapping Impervious Surface Area. *Remote Sensing, 7*, 17168-17189

Liu, X.P., Hu, G.H., Chen, Y.M., Li, X., Xu, X.C., Li, S.Y., Pei, F.S., & Wang, S.J. (2018). High-resolution multi-temporal mapping of global urban land using Landsat images based on the Google Earth Engine Platform. *Remote Sensing of Environment, 209*, 227-239

Lu, D., Moran, E., & Hetrick, S. (2011). Detection of impervious surface change with multitemporal Landsat images in an urban-rural frontier. *ISPRS J Photogramm Remote Sens, 66*, 298-306

Lu, D., & Weng, Q. (2004). Spectral mixture analysis of the urban landscape in Indianapolis with Landsat ETM+ imagery. *Photogrammetric Engineering & Remote Sensing, 70*, 1053-1062

Lu, D., & Weng, Q. (2006). Use of impervious surface in urban land-use classification. *Remote Sensing of Environment, 102*, 146-160

MacGregor-Fors, I. (2011). Misconceptions or misunderstandings? On the standardization of basic terms and definitions in urban ecology. *Landscape and Urban Planning, 100*, 347-349

McFeeters, S.K. (2007). The use of the Normalized Difference Water Index (NDWI) in the delineation of open water features. *International Journal of Remote Sensing, 17*, 1425-1432

Mzid, N., Pignatti, S., Huang, W., & Casa, R. (2021). An analysis of bare soil occurrence in arable croplands for remote sensing topsoil applications. *Remote Sensing, 13*, 474

Piyoosh, A.K., & Ghosh, S.K. (2017). Development of a modified bare soil and urban index for Landsat 8 satellite data. *Geocarto International, 33*, 423-442

Ridd, M.K. (1995). Exploring a V-I-S (vegetation-impervious surface-soil) model for urban ecosystem analysis through remote sensing: comparative anatomy for cities†. *International Journal of Remote Sensing, 16*, 2165-2185

Shao, Z., Huq, M.E., Cai, B., Altan, O., & Li, Y. (2020). Integrated remote sensing and GIS approach using Fuzzy-AHP to delineate and identify groundwater potential zones in semi-arid Shanxi Province, China. *Environmental Modelling & Software, 134*, 104868

Shuster, W.D., Bonta, J., Thurston, H., Warnemuende, E., & Smith, D. (2005). Impacts of impervious surface on watershed hydrology: A review. *Urban Water Journal, 2*, 263-275

Slonecker, E.T., Jennings, D.B., & Garofalo, D. (2001). Remote sensing of impervious surfaces: A review. *Remote Sensing Reviews, 20*, 227-255

Sohn, W., Kim, J.-H., Li, M.-H., Brown, R.D., & Jaber, F.H. (2020). How does increasing impervious surfaces affect urban flooding in response to climate variability? *Ecological Indicators, 118*, 106774

Stathakis, D., Perakis, K., & Savin, I. (2012). Efficient segmentation of urban areas by the VIBI. *International Journal of Remote Sensing, 33*, 6361-6377

Story, M., & Congalton, R.G. (1986). Accuracy assessment: a user's perspective. *Photogrammetric Engineering and Remote Sensing, 52*, 397-399

Sun, G., Chen, X., Jia, X., Yao, Y., & Wang, Z. (2016). Combinational Build-Up Index (CBI) for Effective Impervious Surface Mapping in Urban Areas. *Ieee Journal of Selected Topics in Applied Earth Observations and Remote Sensing, 9*, 2081-2092

Sun, Z., Wang, C., Guo, H., & Shang, R. (2017). A Modified Normalized Difference Impervious Surface Index (MNDISI) for Automatic Urban Mapping from Landsat Imagery. *Remote Sensing, 9*, 18

Van de Voorde, T., Jacquet, W., & Canters, F. (2011). Mapping form and function in urban areas: An approach based on urban metrics and continuous impervious surface data. *Landscape and Urban Planning, 102*, 143-155

Van Deventer, A., Ward, A., Gowda, P., & Lyon, J. (1997). Using thematic mapper data to identify contrasting soil plains and tillage practices. *Photogrammetric Engineering and Remote Sensing, 63*, 87-93

Wang, Y., & Li, M. (2019). Urban Impervious Surface Detection From Remote Sensing Images: A review of the methods and challenges. *Ieee Geoscience and Remote Sensing Magazine, 7*, 64-93

Weng, Q.H. (2012). Remote sensing of impervious surfaces in the urban areas: Requirements, methods, and trends. *Remote Sensing of Environment, 117*, 34-49

Xu, H. (2007). Modification of normalised difference water index (NDWI) to enhance open water features in remotely sensed imagery. *International Journal of Remote Sensing, 27*, 3025-3033

Xu, H. (2008). A new index for delineating built-up land features in satellite imagery. *International Journal of Remote Sensing, 29*, 4269-4276

Xu, H. (2010). Analysis of Impervious Surface and its Impact on Urban Heat Environment using the Normalized Difference Impervious Surface Index (NDISI). *Photogrammetric Engineering & Remote Sensing, 76*, 557-565

Xu, Z., Jiao, L., Lan, T., Zhou, Z., Cui, H., Li, C., Xu, G., & Liu, Y. (2021). Mapping hierarchical urban boundaries for global urban settlements. *International Journal of Applied Earth Observation and Geoinformation, 103*, 102480

Yuan, F., & Bauer, M.E. (2007). Comparison of impervious surface area and normalized difference vegetation index as indicators of surface urban heat island effects in Landsat imagery. *Remote Sensing of Environment, 106*, 375-386

Yue, H., & Liu, Y. (2019). Method for delineating open water bodies based on the deeply clear waterbody delineation index. *Journal of Applied Remote Sensing, 13*, 16

Zha, Y., Gao, J., & Ni, S. (2003). Use of normalized difference built-up index in automatically mapping urban areas from TM imagery. *International Journal of Remote Sensing, 24*, 583-594

Zhang, L.H., Tian, Y.G., & Liu, Q.W. (2021). A Novel Urban Composition Index Based on Water-Impervious Surface-Pervious Surface (W-I-P) Model for Urban Compositions Mapping Using Landsat Imagery. *Remote Sensing, 13*, 20

Zhang, S., Yang, K., Li, M., Ma, Y., & Sun, M. (2018). Combinational biophysical composition index (CBCI) for effective mapping biophysical composition in urban areas. *Ieee Access, 6*, 41224-41237

Zhou, Y., Yang, G., Wang, S., Wang, L., Wang, F., & Liu, X. (2014). A new index for mapping built-up and bare land areas from Landsat-8 OLI data. *Remote Sensing Letters, 5*, 862-871